Active-power control strategies in grid-forming power converters to improve transient stability in power systems with 100% converter-based generation

Régulo E. Ávila-Martínez*†, Luis Rouco*†, Javier Renedo†, Lukas Sigrist*†, Aurelio Garcia-Cerrada*†
* Instituto de Investigación Tecnológica (IIT), Madrid, Spain
{regulo.avila, luis.rouco, aurelio.garcia, lukas.sigrist}@iit.comillas.edu
† ETSI ICAI, Universidad Pontificia Comillas, Madrid, Spain
javier.renedo@ieee.org

***Abstract*—Grid-forming voltage source converters (GFM-VSCs) are among the technologies that play a crucial role in supporting system dynamics. In systems with a high proportion of GFM-VSC-based generation, transient stability becomes a critical limiting factor for stressed power systems. Previous studies have proposed control strategies for GFM-VSCs to improve the transient stability of such systems. These approaches typically rely on suitable current-limiting algorithms, voltage/reactive-power and active-power supplementary control strategies. This paper investigates and compares the effectiveness of three active-power supplementary control strategies to enhance transient stability in multi-converter systems: (i) a wide-area control strategy (TSP-WACS) using the centre of inertia (COI) frequency, (ii) a local transient damping method (TSP-TDM), and (iii) a novel local control strategy (TSP-L) proposed in this work. All strategies were implemented and assessed using short-circuit simulations on Kundur's two-area test system with 100% GFM-VSC generators, demonstrating CCT improvement. The TSP-WACS achieves the best performance but requires a communication infrastructure, while TSP-L offers a simple, robust alternative using only local measurements.**

***Index Terms*—Voltage source converter, VSC, grid forming, transient stability**

I. Introduction

Transient stability has traditionally been associated with the rotor-angle dynamics of synchronous machines [1], [2]. In power systems consisting solely of synchronous generators, this phenomenon is well understood and extensively studied. However, as the use of inverter-based resources continues to increase, the concept of transient stability has gained renewed importance in multi-converter systems. Recent studies have shown that loss of synchronism may also occur in systems dominated by grid-forming converters after large disturbances [3], [4] Consequently, the term transient stability is now also used to describe loss of synchronism phenomena in systems with high or even 100% penetration of non-synchronous generation [5], [6], [7]. Over the past few years, research publications have examined the impact of various control approaches on transient stability in GFM-VSC-based systems [8], [9], [10], [11]. These publications have explored the effects of droop control, current saturation, fault-ride-through capability, and voltage source modulation. Several control strategies have been proposed for GFM-VSC in order to improve transient stability in power systems with 100% GFM-VSC-based generators [12], [13].

The impact of current-limiting mechanisms on transient stability is a well-established and critical area of research in power systems with GFM-VSC converters. Different current-limiting strategies have been proposed to enhance the transient stability margin [14], [15], [16], [17]. The work in [14] introduces the concept of hybrid current limiters (HCLs), proving effective for converter protection and improving transient stability, significantly increasing fault critical clearing times (CCT). Another approach [18] has demonstrated that reactive-power/voltage-based control strategies implemented as fast voltage boosters (FVBs) can significantly improve the transient stability in 100% GFM-VSC systems. The FVBs implement local or global measurements and have demonstrated significant CCT improvements and robustness to realistic communication latencies. Complementarily, the work in [19] showed that FVBs can have further CCTs improvements when they are used with hybrid current limiters (HCLs) [14].

Despite the effectiveness of voltage/reactive-power solutions (FVBs) [18] and combining with hybrid current limiters (HCLs) [19], the direct and precise control of active power remains a key area for further CCT enhancement. Several studies have addressed the direct control of active power as a fundamental mechanism to enhance angle stability. The studies presented in [20], [21] introduce a novel approach to improving the stability of power grids with 100% of GFM-VSC-based generators. The work [20] proposes a P-control strategy, based on a PI controller, that controls the input power of virtual synchronous generators (VSGs). The proposed controller reduces oscillations relative to the frequency of the centre of inertia (COI) using a small signal analysis. The study demonstrates the effectiveness of their method in enhancing the stability of

Submitted to the 24th Power Systems Computation Conference (PSCC 2026).

multi-converter systems. Meanwhile, the paper [21] present the same proposed method, focusing on large disturbances using the frequency deviation with respect to the COI-frequency of the grid as an input signal. Simulation results show that their method efficiently improves both synchronism and damping terms, producing transient stability improvements.

However, these global measurement-based approaches present implementation challenges. In contrast, the research presented in [22] proposes a supplementary P-control strategy to improve transient stability using a transient damping method (TDM) for a GFM-VSC connected to an infinite grid. The P-control method adds a proportional gain to the frequency deviation with respect to the nominal frequency, using local measurements. The TDM strategy changes its active-power set-point proportionally to its frequency deviation through a high-pass filter (HPF), as a solution for stabilising power systems. The study also discusses the limitations of the TDM approach and provides guidelines for the design of the proposed controller in improving transient stability in power systems. Unlike the strategy in [20], which uses global measurements of the centre of inertia to try to pull all VSC frequencies together to join the COI frequency, the TDM control action slows down all the converters independently when they are close to or far from the faults. This means that the TDM control strategy also slows down the converters below the centre of inertia, jeopardising the transient stability.

This analysis highlights a noticeable lack of an effective local active power control strategy for multi-converter systems. While the P-TDM controller proposed in [22] provides a local approach, its application and effectiveness in multi-converter systems remain unproven and are still questionable due to its lack of selectivity regarding fault location. Therefore, there is a need to explore effective P-control strategies in GFM-VSCs to improve transient stability in multi-converter systems, especially when using local measurements.

In this context, this paper proposes a local active-power control strategy (TSP-L), designed to be active only for severe-enough faults in a multi-converter system with 100% GFM-VSC-based generators. The TSP-L control will be only activated for those converters that are close to the faults and disabled for those ones far from the faults. The aim of this design is to mitigate the risks associated with the TSP-TDM strategy without jeopardising system stability.

Furthermore, this work presents a comparative study of three active-power control strategies for improving transient stability in 100% GFM-VSC systems: the wide-area TSP-WACS [21] (which uses the Centre of Inertia frequency), the local TSP-TDM [22] (based on local frequency deviations), and the novel local TSP-L (which activates control actions based on local voltage and frequency thresholds).

By conducting a thorough analysis and comparison of various P-supplementary controllers designed for GFM-VSCs, the main contributions of this study are as follows:

- Proposal of a local active-power control strategy to improve transient stability of power systems with 100% of GFM-VSC-based generation.
- Comparison of the proposed control strategy with two existing strategies based on both global measurements (TSP-WACS) and local measurements (TSP-TDM).
- Demonstration, via simulations, of the effectiveness of the control approaches in significantly improving the critical clearing times of different faults.
- Analysis of the impact of communication latency on the global control strategy (TSP-WACS), showing that the proposed control strategy is robust for realistic communication delays.

The performance of the control strategies is demonstrated through simulation using Kundur's two-area test system [23] with 100% grid-forming VSC-based generation.

II. Grid-forming VSCs

A. Modelling and control

The equivalent circuit model for a GFM-VSC, following the established methodology in [24], [25], [26] , is described in this section. As depicted in Fig. 1, the GFM-VSC-i converter is modeled as a voltage source ($\bar{e}_{m,i}$) connected to the rest of the system through an LC filter, consisting of a phase reactor ($\bar{z}_{f,i} = r_{f,i} + j\omega_i L_{f,i}$) and a capacitor ($\bar{z}_{Cf,i} = -j/(\omega_i C_{f,i})$), and a transformer ($\bar{z}_{c,i} = r_{c,i} + j\omega_i L_{c,i}$).

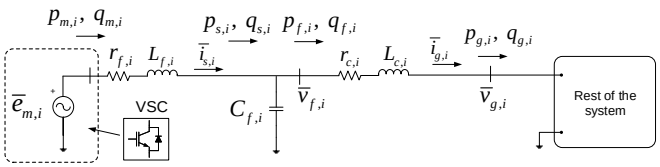


Fig. 1. Model of a grid-forming VSC.

Fig. 4 displays the general control scheme for GFM-VSC-i, [25]. The scheme consist of a cascade AC voltage and current control loops operating in the $d-q$ reference frame: (a) a voltage controller, (b) a virtual transient resistance to enhance damping during disturbances [25], (c) a current controller with current limitation, and (d) voltage modulation with modulation index limitations. Finally, (e) a Virtual Synchronous Machine (VSM) control mechanism (to enable the GFM-VSCs self-synchronization capability) [24], [25].

The GFM-VSC-i controls voltage magnitude $v_{f,i}$ and frequency $\omega_{f,i}$ (and, thus, the voltage angle $\delta_{f,i}$) at bus f_i. The angle $\delta_{f,i}$ (rad) is imposed by the GFM-VSC VSM control (e) (Subection II-B), aligning $\bar{v}_{f,i}$ with the direct axis component (d-axis) of the rotating $d-q$ reference frame.

B. Virtual synchronous machine control (VSM)

The virtual synchronous machine (VSM) control is used as a self-synchronisation mechanism in the GFM-VSC as is shown in Fig. 2 [27], [21].

The swing equation emulated by a VSM is given by:

$$2H_{VSC,i}\frac{d\Delta\omega_i}{dt} = p^0_{g,i} - p_{g,i} - D_{VSC,i}\Delta\omega_i \quad (1)$$

where:

- $H_{VSC,i}$ (s) is the emulated inertia constant.
- $D_{VSC,i}$ (pu) is the proportional gain of the primary frequency response (PFR). It also plays the role of damping coefficient.
- $\Delta\omega_i = \omega_i - \omega_{0,pu}$ (pu), where ω_i is the frequency imposed by the GFM-VSC and $\omega_{0,pu} = 1$ pu.
- $p^0_{g,i}$ (pu) is a constant active-power set-point of the GFM-VSC at the connection point.
- $p_{g,i}$ (pu) is the active-power injected by the GFM-VSC at the connection point.
- ω_0 is the nominal frequency in rad/s.

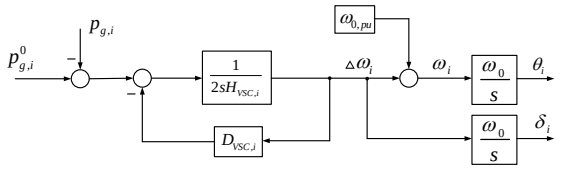


Fig. 2. VSM control in a GFM-VSC.

Through equation (1), the GFM-VSC-i controls the frequency ω_i (pu) at its connection point (bus f_i). Fig. 2 shows the angles used for the Park's Transformation applied in the control loops (see Fig. 4).

III. Active-Power control strategies

This section describes three active-power control strategies in GFM-VSC with VSM control. One of these strategies uses global measurements that consider the frequency of the centre of inertia (COI), and the other two strategies use local measurements, one of which is the novel contribution of this work. Both global and local approaches have shown improvements in transient stability.

The three control strategies analysed in this section are:

- Active-power control using a wide-area control system (**TSP-WACS**) [21] that uses the frequency of the centre of inertia (COI) as a reference..
- Local Active-power control using transient damping method (**TSP-TDM**) [22] that sets the power setpoint based on local frequency deviations.
- A novel local Active-power control (**TSP-L**) strategy proposed in this work, which activates control actions based on local voltage and frequency thresholds.

During a fault event, the voltage at the connection point ($v_{g,i}$) decreases, leading to a reduction in active power injection ($p_{g,i}$) according to Eq. (2):

$$p_{g,i} \simeq \frac{v_{f,i} v_{g,i}}{x_{c,i}} \sin(\delta_{f,i} - \delta_{g,i}) \tag{2}$$

where $p_{g,i}$ is the electrical active power of the converter; $v_{f,i}$ and $v_{g,i}$ are the voltage magnitudes at bus f_i and the PCC (g_i), respectively; $x_{c,i}$ is the coupling reactance; and $\delta_{f,i}$ and $\delta_{g,i}$ are the corresponding power angles of $v_{f,i}$ and $v_{g,i}$.

The TSP strategies inject a supplementary active power reference, $\Delta p^{ref,TS}_{g,i}$, into the primary power set-point of the converter:

$$p^{ref}_{g,i} = p^0_{g,i} + \Delta p^{ref,TS}_{g,i} \tag{3}$$

where:

- $p^{ref}_{g,i}$ is the final active power reference for the converter.
- $p^0_{g,i}$ is the active power reference from the primary controller (e.g., VSM).
- $\Delta p^{ref,TS}_{g,i}$ is the supplementary control action applied to the primary power set-point for transient Stability.

A. Active-power control using a wide-area control system (TSP-WACS) [21]

Fig. 3 shows the TSP-WACS strategy proposed in [21] to improve transient stability, aiming to converge the frequencies of all converters toward the centre of inertia (COI) frequency (ω_{COI}) of the system. According to the GFM-VSC's emulated swing equation, this power reduction results in an acceleration of the converter. In a multi-converter system, the severity of the voltage drop varies with fault distance:

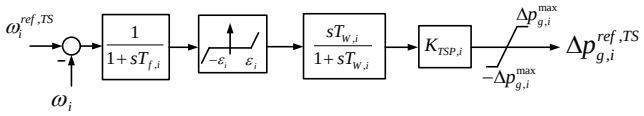


Fig. 3. Strategy TSP-WACS.

- GFM-VSCs closer to the fault experience a more severe voltage drop, accelerating more significantly and resulting in a frequency above the COI frequency ($\omega_i > \omega_{COI}$).
- GFM-VSCs located farther from the fault accelerate less, potentially operating below the COI frequency ($\omega_i < \omega_{COI}$).

The objective of the TSP-WACS is to manage the active power to pull the frequencies of all converters towards ω_{COI}, thereby mitigating the risk of loss of synchronism among them. The control action of Fig. 3 ($\Delta p^{ref,TS}_{g,i}$) is determined based on the deviation of the local frequency (ω_i) from the COI frequency (ω_{COI}):

- For accelerated converters ($\omega_i > \omega_{COI}$): if the frequency of VSC-i is above the frequency of the COI, TSP-WACS injects a negative supplementary active power reference ($\Delta p^{ref,TS}_{g,i} < 0$) to slows down the converters.
- For lagging converters ($\omega_i < \omega_{COI}$): if the frequency of VSC-i is below the frequency of the COI, TSP-WACS injects a positive supplementary active power reference ($\Delta p^{ref,TS}_{g,i} > 0$) to slightly accelerate the GFM-VSC towards the COI frequency.
- In this way, control actions will pull together the frequencies of GFM-VSCs of the system.

As this strategy involves calculating and using the ω_{COI} measurement, a Wide-Area Control System (WACS) is required for the communication sysytem.

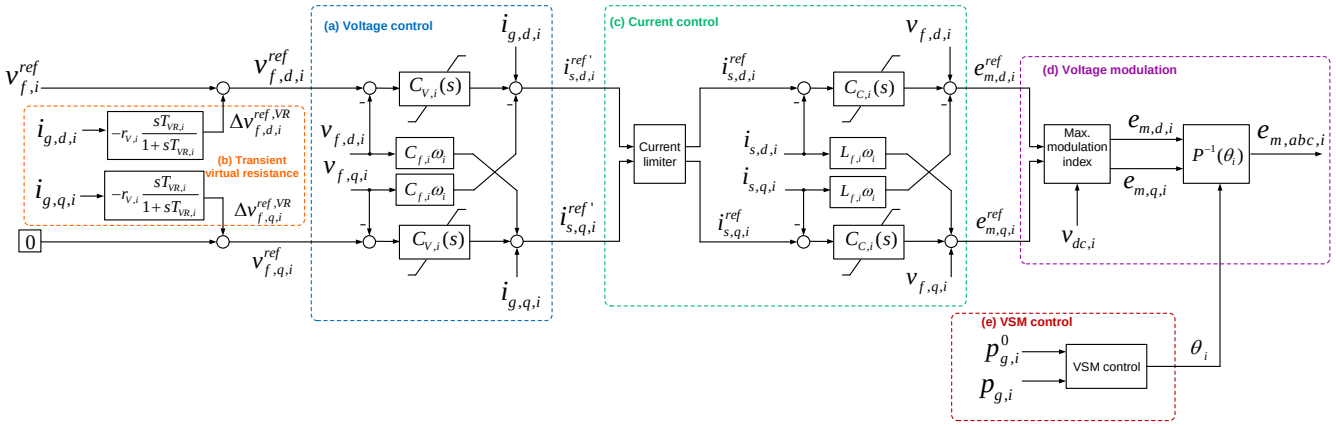


Fig. 4. General scheme of the control system of a grid-forming VSC.

B. Local Active-power control using transient damping method (TSP-TDM) [22]

This control strategy consists of a transient damping method in VSM proposed in [22] for transient stability improvement in GFM-VSCs connected to infinite gird. The input of the controller of TSP-TDM is the frequency deviation of each GFM-VSC-i, with respect to an absolute reference frequency, $\Delta\omega_i = \omega_i - \omega_{0,pu}$. Fig. 5 shows the scheme of the TDM implemented in a GFM-VSC with VSM control.

The TDM control strategy consists of a gain ($K_{TSP,i}$) and a wash-out filter (with a time constant of $T_{W,i}$). Although not discussed in [22], this work includes a saturation parameter to limit the contribution of control actions (such as the TSP-L and TSP-WACS controllers) for a fair comparison, denoted as $\pm\Delta p_{g,i}^{max}$. The controller takes the frequency deviation ($\Delta\omega_i$) calculated by the VSM algorithm of the GFM-VSC as input, and its output is a supplementary active-power set point ($\Delta p_{g,i}^{ref,TS}$). In the TDM control strategy, each GFM-VSC adds a supplementary active-power set point that is proportional to the frequency deviation, which uses only local information.

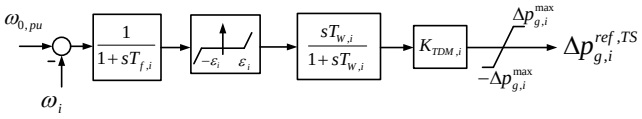


Fig. 5. Strategy TSP-TDM.

In contrast to the TSP-WACS, which uses global measurements of the centre of inertia to try to pull all VSC frequencies together to join the COI frequency, the TDM control action slows down all the converters independently when they are close to or far from the faults. This means that the TDM control strategy also slows down the converters below the centre of inertia, which would jeopardise the transient stability.

C. Propose Local Active-power control (TSP-L)

This Section introduces the proposed local active-power (TSP-L) control strategy applying a supplementary active power setpoint, $\Delta p_{g,i}^{ref,TS}$, to the power reference as shown in the block diagram in Fig. 6. The TSP-L uses two primary input signals: the terminal voltage ($v_{g,i}$) and the frequency deviation ($\Delta\omega_i$) of the GFM-VSC-i. This combination of inputs is used to create a selective activation mechanism. By monitoring the local voltage and frequency, the TSP-L ensures that the supplementary active power control is only triggered when critical fault thresholds are reached. TSP-L is activated when the voltage at the connection point is lower than a certain threshold and it remains activated if the frequency difference is greater than a certain threshold ($v_{A,i}$, $v_{B,i}$ and $\omega_{thres,i}$).

The activation philosophy for the TSP-L strategy shown in Figs. 6 and 7 is as follows:

- Binary variable $\gamma_{1,i}$ is set to 1 if a voltage sag is detected with an hysteresis, as shown in Fig. 6. If $v_{g,i} \leq v_{A,i}$, then $\gamma_{1,i} = 1$ and remains equal to 1 until $v_{g,i} > v_{B,i}$. if a fault is not detected, then $\gamma_{1,i} = 0$.
- Binary variable $\gamma_{2,i}$ is set to 1 if the frequency deviation of GFM-VSC-i (with respect to the nominal frequency) is greater than or equal to a certain threshold: $\Delta\omega_i \geq \omega_{thres,i}$. Otherwise, $\gamma_{2,i} = 0$.
- The supplementary controller is activated with binary variable γ_i, which is the result of a logic circuit with $\gamma_{1,i}$ and $\gamma_{2,i}$ as inputs, as shown in Fig. 6.
- The supplementary active-power set point is given by: $\Delta p_{g,i}^{ref,TS} = \gamma_i \Delta p_{g,i}^{max}$, where $\Delta p_{g,i}^{max} > 0$ is a parameter of the controller ($\gamma_i = 0$ if the controller is deactivated and $\gamma_i = 1$ if the controller is activated).

The logic used to activate the controller can then be summarised as follows:

- The controller will be activated if a voltage sag is detected. Therefore, $\gamma_{1,i}$ will drive the activation of the controller.
- Once the controller is activated, the supplementary active-power set-point is maintained if at least one of the two following conditions are satisfied: undervoltage ($\gamma_{1,i} = 1$) or frequency greater than or equal to the threshold ($\gamma_{2,i} = 1$).

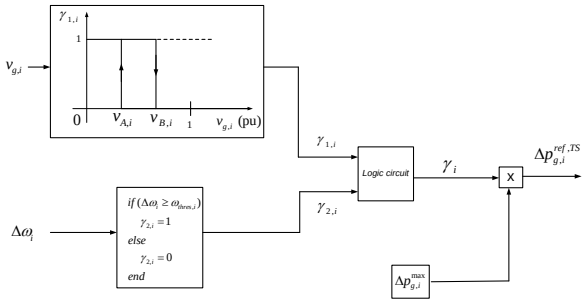


Fig. 6. Strategy TSP-L.

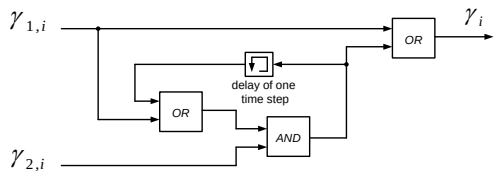


Fig. 7. Strategy TSP-L. Logic circuit for fault detection.

Unlike TSP-TDM, which activates the control more broadly, the key difference with TSP-L lies in its activation logic, which has conditioned action rules. This ensures that the control is only activated during several-enough faults, guaranteeing that supplementary active power is applied only to the converters that require it within the multi-converter environment.

IV. Results and Simulation Analysis

This section assesses the three supplementary P-control strategies by analyzing the system's transient stability. The analysis is performed on Kundur's two-area test system [28], where the original synchronous machines have been replaced by 100% grid-forming VSC-based generation, as illustrated in Fig. 8. The GFM-VSCs-based generators operate using VSM control and maintain the same nominal apparent power (900 MVA) as the original synchronous generators. System data and GFM-VSCs parameters are detailed in the Appendix (Table VI). [1]

Four cases are compared:

- Base case: no supplementary controller for transient stability is implemented in the GFM-VSCs.
- TSP-L: VSCs applying TSP-L strategy (Figs. 6 and 7), with parameters: $v_{A,i} = 0.50$ pu, $v_{B,i} = 0.9$ pu, $\omega_{thres,i} = 10^{-3}$ pu, $\Delta p_{g,i}^{max} = 0.15$ pu.
- TSP-WACS: VSCs applying TSP-WACS strategy (Fig. 3), with parameters: $K_{TSP,i} = 100$ pu, $T_{f,i} = 0.1$ s, $T_{W,i} = 10$ s, $\Delta p_{g,i}^{max} = 0.15$ pu and $\epsilon_i = 10^{-3}$ pu.
- TSP-TDM: VSCs applying TSP-TDM strategy (Fig. 5) with parameters: $K_{TSP,i} = 100$ pu, $T_{f,i} = 0.1$ s, $T_{W,i} = 10$ s, $\Delta p_{g,i}^{max} = 0.15$ pu and $\epsilon_i = 10^{-3}$ pu.

[1]Simulations were conducted using average electromagnetic-type models within the VSC_Lib tool, an open-source library based on Matlab + Simulink + SimPowerSystems [29].

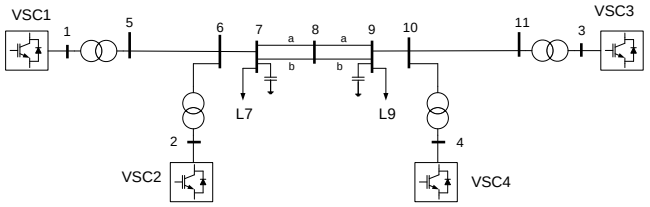


Fig. 8. Kundur's two-area test system with 100 % GFM-VSC-based generation.

A. Short-circuit simulation

Fault I (Table I) is applied at $t = 1$ s and cleared after 150 ms. As shown in Fig. 9 (angle difference between VSC-1 and VSC-3), VSC-based generators lose synchronism in the Base Case. However, synchronism is successfully maintained when any of the three supplementary controllers (TSP-L, TSP-TDM, and TSP-WACS) are implemented.

TABLE I
Fault Description.

	Short circuit at line $i-j$	close to bus	clearing
Fault I	7-8a	7	Disconnect 7-8a
Fault II	5-6	5	short circuit cleared (line not disconnected)
Fault III	10-11	11	short circuit cleared (line not disconnected)
Fault IV	8-9a	8	Disconnect 8-9a

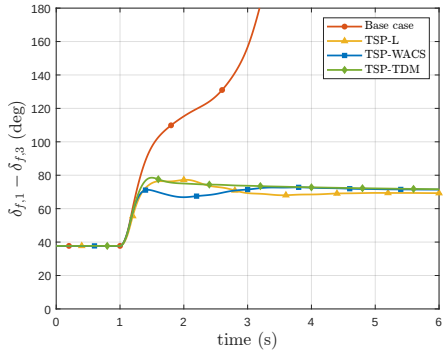


Fig. 9. Fault I cleared after 150 ms. Angle difference of the VSCs applying TSP controllers.

Fig. 10 shows the frequency deviations of the VSCs with respect to the COI frequency. The TSP-L strategy, illustrated in Fig. 11, demonstrates its selective activation: the supplementary active-power set-point ($\Delta P_g^{ref,TS}$) is only provided to VSCs 1 and 2 (close to the fault), and not to VSCs 3 and 4 (distant from the fault). This is the result of the activation logic (Fig. 7). In contrast, the TSP-TDM strategy activates in all converters, using local frequency deviation from nominal frequency ($\omega_{0,pu} = 1$ pu). Since all VSCs accelerate during the fault (i.e., $\omega_i > \omega_{0,pu}$), the TSP-TDM action aims to decelerate all of them simultaneously.

The TSP-WACS strategy provides the most coordinated action: VSCs 1 and 2 ($\omega_i > \omega_{COI}$) receive a negative supplementary power set-point to slow down the converters,

while VSCs 3 and 4 ($\omega_i < \omega_{COI}$) receive a positive set-point to accelerate the GFM-VSCs (Fig. 10 and 11). This coordinated control effectively reduces the angle difference and mitigates the risk of loss of synchronism.

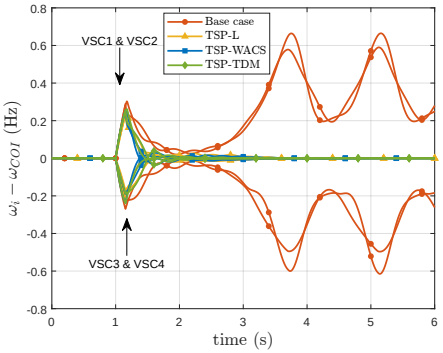


Fig. 10. Fault I cleared after 150 ms. Frequency deviations of the VSCs with respect to the frequency of the COI applying TSP controllers.

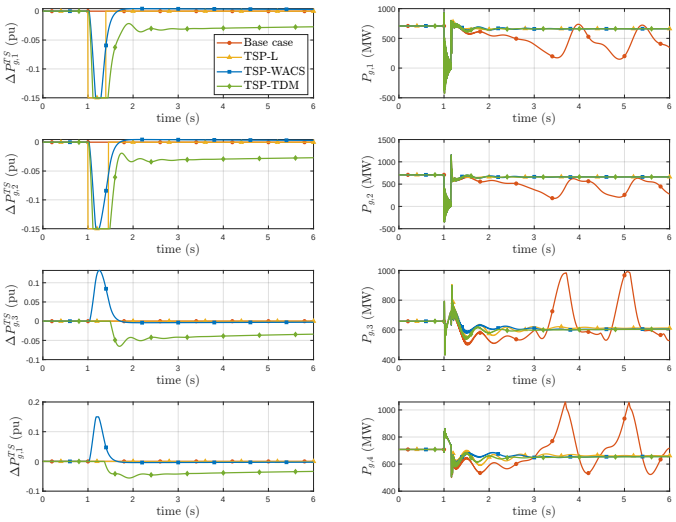


Fig. 11. Fault I cleared after 150 ms. (left) Active-power set-points and (right) active-power injections of each VSC applying TSP controllers.

B. Critical clearing times (CCTs)

The CCTs for the fault scenarios described in Table I are presented in Table II. All three P-supplementary control strategies (TSP-L, TSP-TDM, and TSP-WACS) were implemented in all GFM-VSCs of Fig. 8 and were found to significantly increase the CCTs compared to the base case. A washout-filter time constant of $T_{W,i} = 10$ s was selected for the TSP-TDM and TSP-WACS strategies, with a proportional gain of $K_{TSP,i} = 100$ pu. Additionally, the supplementary active-power set point for all strategies was limited to a practical value of $\Delta p_{g,i}^{max} = 0.15$ pu.

As Table II illustrates, the effectiveness of the strategies varies by fault type. For instance, the TSP-WACS strategy yields the best performance for Fault I and Fault II. The TSP-TDM strategy also achieves good CCTs, reaching a competitive performance for Fault II. However, the TSP-L strategy, with its dependency on the voltage activation threshold ($v_{A,i}$), shows the most robust increase in CCTs for Faults I, II, and III.

The performance for Fault IV highlights a key design difference. The Base Case CCT for Fault IV is notably lower, and the TSP-L strategy, when implemented with $v_{A,i} = 0.75$ pu, leads to a reduction in the CCT (from 420 ms to 300 ms, as shown in the table). This adverse effect is mitigated by setting the threshold to a lower value, $v_{A,i} = 0.5$ pu, which maintains the base case CCT of 420 ms. This demonstrates the importance of the TSP-L's selective activation, ensuring that the control action only engages for severe faults near the converter without jeopardizing stability elsewhere. Therefore, $v_{A,i} = 0.5$ pu is adopted as the optimal setting for the TSP-L strategy.

TABLE II
CRITICAL CLEARING TIMES (CCTS) FOR TSPS.

CCT (ms)	base case	TSP-L $v_{A,i} = 0.75$ pu	TSP-L $v_{A,i} = 0.5$ pu	TSP-TDM	TSP-WACS $\tau = 0$ ms	with 50 ms	delay 100 ms
Fault I	130	300	300	230	280	270	270
Fault II	270	390	390	350	430	410	390
Fault III	220	260	260	240	320	300	270
Fault IV	420	300	420	540	1520	1420	1410

C. Impact of the activation of the TSP controllers in different areas.

To evaluate the impact of fault location and control selectivity, Tables III and IV present the CCTs when the supplementary control strategies are activated only in Area 1 or Area 2, respectively.

TABLE III
CRITICAL CLEARING TIMES (CCTS) FOR TSPS. AREA 1

CCT (ms)	base case	TSP-L $v_{A,i} = 0.5$ pu	TSP-TDM $K_{TSP,i} = 100$ pu	TSP-WACS $K_{TSP,i} = 100$ pu
Fault I	130	300	270	230
Fault II	270	390	360	350
Fault III	220	220	220	320
Fault IV	420	420	1080	840

TABLE IV
CRITICAL CLEARING TIMES (CCTS) FOR TSPS. AREA 2

CCT (ms)	base case	TSP-L $v_{A,i} = 0.5$ pu	TSP-TDM $K_{TSP,i} = 100$ pu	TSP-WACS $K_{TSP,i} = 100$ pu
Fault I	130	130	0	230
Fault II	270	270	250	350
Fault III	220	260	250	610
Fault IV	420	420	0	790

In Area 1, all strategies demonstrate a clear improvement over the Base Case for faults I and II. Specifically, the TSP-TDM and TSP-WACS strategies achieve substantial CCT increases for Fault IV, underscoring the potential of active power control when a fault is physically distant from the converters being controlled (Area 1 VSCs are far from Fault IV). Conversely, the TSP-L strategy, designed for selective activation, maintains the Base Case CCT for Fault IV, confirming that its logic successfully prevents unnecessary control action for less critical disturbances.

The analysis of Area 2 (Table IV) reveals a critical drawback of the TSP-TDM strategy. While TSP-WACS consistently improves CCTs across all four fault scenarios, the TSP-L strategy

is correctly inactive for Faults I, II, and IV, maintaining Base Case performance, but successfully increases the CCT for Fault III. More significantly, the TSP-TDM strategy results in a CCT of **0** ms for Faults I and IV. A CCT of 0 ms indicates that the control action itself destabilizes the system following even a minimal fault clearance time, demonstrating that the non-selective action of TSP-TDM in this multi-converter system.

D. Impact of communication latency

It is essential to analyze the influence of communication latency on the performance of the TSP-WACS strategy, as it relies on a Wide-Area Control System (WACS). To model this, the input error signal of the supplementary controller in Fig. 3 is subjected to a communication delay (τ), as shown:

$$u_i = e^{-s\tau}(\omega_{COI} - \omega_i) \tag{4}$$

Previous studies on WACS report delays ranging from 50 to 80 ms [30]. Based on this, we analyze the TSP-WACS strategy using conservative delays of 50 ms and 100 ms.

The results, presented in Table V, demonstrate that the TSP-WACS strategy is highly robust against realistic communication latency. While an increase in τ naturally leads to a slight reduction in CCTs across various fault scenarios, the strategy consistently maintains the best overall performance compared to TSP-L and TSP-TDM (see Table II for comparison).

TABLE V
CRITICAL CLEARING TIMES (CCTS) FOR TSP-WACS WITH DELAY.

CCT (ms)	**TSP-WACS** with delay $\tau = 0$ ms	50 ms	100 ms
Fault I	280	270	270
Fault II	430	410	390
Fault III	320	300	270
Fault IV	1520	1420	1410

E. Discussion on the use of the three P control strategies

The choice among the three supplementary active power controllers depends primarily on the trade-off between implementation complexity (cost and infrastructure) and transient performance (CCTs). The TSP-L and TSP-TDM strategies utilize only local measurements, making them easier and more cost-effective to implement as they avoid the need for a Wide-Area Control System (WACS) and its associated communication infrastructure. Conversely, the TSP-WACS strategy relies on global measurements, adding complexity and cost due to the required communication system, though it provides the best performance.

In terms of effectiveness, the TSP-WACS strategy, which references the Center of Inertia (COI) frequency, achieves the best results (CCT improvements). This is because it aligns the control action with the ideal response: injecting negative power to accelerating VSCs ($\omega_i > \omega_{COI}$) and positive power to slow down VSCs ($\omega_i < \omega_{COI}$). The local strategies, TSP-L and TSP-TDM, approximate this ideal action using local frequency deviations from nominal frequency. A key advantage of the novel TSP-L strategy over TSP-TDM is its selective activation mechanism. By tuning the voltage and frequency thresholds, TSP-L ensures the controller only engages for severe, nearby faults that genuinely jeopardize stability. This selectivity prevents the unnecessary intervention observed in the TSP-TDM strategy, which can adversely affect CCTs for remote faults.

In conclusion, while the TSP-WACS strategy is superior in maximizing CCT and is robust against latency, its deployment is limited by communication requirements. The local TSP-TDM provides simplicity but lacks control selectivity. The proposed TSP-L strategy offers the optimal balance, providing robust CCT improvements comparable to TSP-WACS for key fault types, but achieving this without any communication overhead. Therefore, TSP-L is the most practical choice for enhancing transient stability in systems where the implementation of a WACS is unfeasible.

V. CONCLUSIONS

This paper investigated three supplementary active power control (P-control) strategies (TSP-WACS, TSP-TDM, and the novel TSP-L) to enhance the transient stability of 100% GFM-VSCs-based power systems. A direct comparison of local versus global approaches was provided, including an analysis of TSP-WACS sensitivity to communication latency and design guidelines for TSP-L.

The key conclusions derived from the analysis and simulation results are as follows:

- The TSP-WACS strategy, which utilizes global measurements (COI frequency), achieved the best overall performance by effectively coordinating the frequency of all converters, significantly increasing Critical Clearing Times (CCTs).
- While the local TSP-TDM method improved transient stability for close faults, its non-selective action on fault location demonstrated risks in multi-converter systems, potentially jeopardizing stability.
- The proposed TSP-L strategy successfully overcomes the limitations of TSP-TDM by implementing an activation logic based on local voltage and frequency thresholds. This selectivity ensures the controller acts only for critical faults, establishing TSP-L as a robust, communication-free alternative for CCT enhancement.
- Design guidelines were provided for parameter tuning, emphasizing that excessive control gains or saturation limits can jeopardize stability. Furthermore, the superior performance of TSP-WACS is heavily dependent on the communication infrastructure, highlighting the practical advantage of the local TSP-L approach.

APPENDIX: DATA

Table VI depicts the data of the grid-forming VSCs. The data of the original two-area Kundur's test system can be found in [28]. In this work the same conditions of [18] were considered: (Load at bus 7: 917 MW & 100 MVAr; load at bus 9: 1817 MW & 100 MVAr). Nominal frequency is 50 Hz.

TABLE VI
PARAMETERS OF THE VSCS

Parameters VSC's rating are base values for pu	
Rating VSC, DC voltage, AC voltage	900 MVA, 640 kV, 300 kV
Max. modulation index ($m_i^{max} = \sqrt{\frac{3}{2}} \cdot \frac{V_{dc,B}}{2V_{ac,B}}$)	1.31 pu
Series filter resistance ($r_{f,i}$)/reactance ($x_{f,i}$)	0.005 pu / 0.15 pu
Shunt filter capacitance ($C_{f,i}$)	0.0660 pu
Transformer resistance ($r_{c,i}$)/reactance ($x_{c,i}$) (900 MVA 300/220 kV transformer)	0.005 pu / 0.15 pu
Current prop./int. control ($K_{C,P,i}$/$K_{C,I,i}$)	0.73 pu / 1.19 pu/s
Voltage prop./int. control ($K_{V,P,i}$/$K_{V,I,i}$)	0.52 pu / 1.16 pu/s
Virtual transient resistance ($r_{V,i}$/$T_{VR,i}$)	0.09 pu / 0.0167 s
Emulated inertia ($H_{VSC,i}$) of VSCs 1, 2, 3 & 4	4.5 s / 4.5 s / 4.175 s / 6.175 s
Damping constant factor gain. ($D_{VSC,i}$)	20 pu

REFERENCES

[1] P. Kundur, J. Paserba, V. Ajjarapu, G. Andersson, A. Bose, C. Canizares, N. Hatziargyriou, D. Hill, A. Stankovic, C. Taylor, T. Van Cutsem, and V. Vittal, "Definition and classification of power system stability IEEE/CIGRE joint task force on stability terms and definitions," *IEEE Transactions on Power Systems*, vol. 19, no. 3, pp. 1387–1401, 2004.

[2] N. Hatziargyriou, J. V. Milanović, C. Rahmann, V. Ajjarapu, C. Canizares, I. Erlich, D. Hill, I. Hiskens, I. Kamwa, B. Pal, P. Pourbeik, J. J. Sanchez-Gasca, A. Stanković, T. Van Cutsem, V. Vittal, and C. Vournas, "Definition and classification of power system stability - revisited and extended," *IEEE Transactions on Power Systems*, vol. 36, no. 4, pp. 3271–3281, 2021.

[3] Y. Wang, Y. Zhou, K. Zhou, T. Wang, Z. Xu, and X. Li, "Study on Transient Stability of Power System Containing Non-Synchronous Machine Sources Based on PSCAD/EMTDC," in *2020 4th International Conference on HVDC (HVDC)*, Nov. 2020, pp. 276–281.

[4] H. Amano and A. Yokoyama, "Rotor Angle Stability Analysis Using Normal form Method with High Penetrations of Renewable Energy Sources-Energy Index for Multi-Swing Stability," in *2018 Power Systems Computation Conference (PSCC)*, Jun. 2018, pp. 1–6.

[5] W. Du, K. P. Schneider, F. K. Tuffner, Z. Chen, and R. H. Lasseter, "Modeling of Grid-Forming Inverters for Transient Stability Simulations of an all Inverter-based Distribution System," in *2019 IEEE Power & Energy Society Innovative Smart Grid Technologies Conference (ISGT)*, Feb. 2019, pp. 1–5.

[6] X. Zhao and D. Flynn, "Transient Stability Enhancement with High Shares of Grid-Following Converters in a 100% Converter Grid," in *2020 IEEE PES Innovative Smart Grid Technologies Europe (ISGT-Europe)*, Oct. 2020, pp. 594–598.

[7] X. He, S. Pan, and H. Geng, "Transient Stability of Hybrid Power Systems Dominated by Different Types of Grid-Forming Devices," *IEEE Transactions on Energy Conversion*, vol. 37, no. 2, pp. 868–879, Jun. 2022.

[8] Z. Shuai, C. Shen, X. Liu, Z. Li, and Z. J. Shen, "Transient angle stability of virtual synchronous generators using lyapunov's direct method," *IEEE Transactions on Smart Grid*, vol. 10, no. 4, pp. 4648–4661, 2018.

[9] H. Cheng, Z. Shuai, C. Shen, X. Liu, Z. Li, and Z. J. Shen, "Transient angle stability of paralleled synchronous and virtual synchronous generators in islanded microgrids," *IEEE Transactions on Power Electronics*, vol. 35, no. 8, pp. 1019–1033, 2020.

[10] D. Pan, X. Wang, F. Liu, and R. Shi, "Transient stability of voltage-source converters with grid-forming control: A design-oriented study," *IEEE Journal of Emerging and Selected Topics in Power Electronics*, vol. 8, no. 2, pp. 1019–1033, 2020.

[11] M. Eskandari and A. V. Savkin, "On the impact of fault ride-through on transient stability of autonomous microgrids: Nonlinear analysis and solution," *IEEE Transactions on Smart Grid*, pp. 1–12, 2020.

[12] X. Zhao and D. Flynn, "Freezing Grid-Forming Converter Virtual Angular Speed to Enhance Transient Stability Under Current Reference Limiting," in *2020 IEEE 21st Workshop on Control and Modeling for Power Electronics (COMPEL)*, ser. ISSN: 1093-5142, Nov. 2020, pp. 1–7.

[13] ——, "Grid-Forming Converter Angular Speed Freezing to Enhance Transient Stability in 100% Grid-Forming and Mixed Power Systems," *IFAC-PapersOnLine*, vol. 55, no. 9, pp. 425–430, 2022.

[14] T. Qoria, F. Gruson, F. Colas, G. Denis, T. Prevost, and X. Guillaud, "Critical clearing time determination and enhancement of grid-forming converters embedding virtual impedance as current limitation algorithm," *IEEE Journal of Emerging and Selected Topics in Power Electronics*, vol. 8, no. 2, pp. 1050–1061, 2020.

[15] E. Rokrok, T. Qoria, A. Bruyere, B. Francois, and X. Guillaud, "Transient stability assessment and enhancement of grid-forming converters embedding current reference saturation as current limiting strategy," *IEEE Transactions on Power Systems*, vol. 37, no. 2, pp. 1519–1531, 2022.

[16] T. Qoria, X. Wang, and R. Kadri, "Grid-forming control vsc-based including current limitation and re-synchronization functions to deal with symmetrical and asymmetrical faults," *Electric Power Systems Research*, vol. 223, p. 109647, 2023. [Online]. Available: https://www.sciencedirect.com/science/article/pii/S0378779623005369

[17] N. Baeckeland, B. Yang, and G.-S. Seo, "Transient stability-enhancing method for grid-forming inverters under current limiting," *IEEE Transactions on Power Electronics*, vol. 40, no. 5, pp. 6714–6725, 2025.

[18] R. E. Ávila Martínez, J. Renedo, L. Rouco, A. García-Cerrada, L. Sigrist, T. Qoria, and X. Guillaud, "Fast voltage boosters to improve transient stability of power systems with 100% of grid-forming VSC-Based generation," *IEEE Transactions on Energy Conversion*, vol. 37, no. 4, pp. 1–11, 2022.

[19] R. E. Ávila-Martínez, J. Renedo, L. Rouco, A. Garcia-Cerrada, L. Sigrist, X. Guillaud, and T. Qoria, "Impact of current limiters and fast voltage boosters in grid-forming vsc-based generators on transient stability," *Electric Power Systems Research*, vol. 235, p. 110753, 2024.

[20] M. Choopani, S. Hosseinain, and B. Vahidi, "A novel comprehensive method to enhance stability of multi-VSG grids," *International Journal of Electrical Power & Energy Systems*, vol. 104, pp. 502–514, 2019.

[21] M. Choopani, S. H. Hosseinian, and B. Vahidi, "New transient stability and LVRT improvement of multi-VSG grids using the frequency of the center of inertia," *IEEE Transactions on Power Systems*, vol. 35, no. 1, pp. 527–538, 2020.

[22] X. Xiong, C. Wu, P. Cheng, and F. Blaabjerg, "An optimal damping design of virtual synchronous generators for transient stability enhancement," *IEEE Transactions on Power Electronics*, vol. 36, no. 10, pp. 11 026–11 030, 2021.

[23] P. Kundur, *Power system stability and control*. McGraw Hill, 1994.

[24] M. Paolone, T. Gaunt, X. Guillaud, M. Liserre, S. Meliopoulos, A. Monti, T. Van Cutsen, V. Vittal, and C. Vournas, "Fundamentals of power systems modelling in the presence of converter-interfaced generation," *Electric Power Systems Research*, vol. 189, no. 106811, pp. 1–33, 2020.

[25] T. Qoria, E. Rokrok, A. Bruyere, B. Francois, and X. Guillaud, "A PLL-Free grid-forming control with decoupled functionalities for high-power transmission system applications," *IEEE access*, no. 106765, pp. 197 363–197 378, 2020.

[26] G. S. Pereira, V. Costan, A. Bruyére, and X. Guillaud, "Simplified approach for frequency dynamics assessment of 100% power electronics-based systems," *Electric Power Systems Research*, vol. 188, no. 106551, pp. 1–8, 2020.

[27] S. D'Arco, J. A. Suul, and O. B. Fosso, "A Virtual Synchronous Machine implementation for distributed control of power converters in SmartGrids," *Electric Power Systems Research*, vol. 122, pp. 180–197, 2015.

[28] P. Kundur, *Power system stability and control*. McGraw Hill Education, New York, NY, USA, 1994.

[29] L2EP-LILLE, "VSC_lib: Grid forming models for Matlab/SimPowerSystem," vol. https://github.com/l2ep-epmlab/ (accessed 08-07-2020), 2020.

[30] F. Zhang, Y. Sun, L. Cheng, X. Li, J. H. Chow, and W. Zhao, "Measurement and modeling of delays in wide-area closed-loop control systems," *IEEE Transactions on Power Systems*, vol. 30, no. 1, pp. 2426–2433, 2015.